

## Reentrant onset of chaos in tubular image states

Dvira Segal

*Department of Chemical Physics, The Weizmann Institute of Science, 76100 Rehovot, Israel; Department of Chemistry, University of British Columbia, Vancouver V6T1Z1, Canada; and Department of Physics, University of British Columbia, Vancouver V6T1Z1, Canada*

Petr Král

*Department of Chemistry, University of British Columbia, Vancouver V6T1Z1, Canada; Department of Physics, University of British Columbia, Vancouver V6T1Z1, Canada; and Department of Chemistry, University of Illinois at Chicago, Chicago, Illinois*

Moshe Shapiro

*Department of Chemical Physics, The Weizmann Institute of Science, 76100 Rehovot, Israel; Department of Chemistry, University of British Columbia, Vancouver V6T1Z1, Canada; and Department of Physics, University of British Columbia, Vancouver V6T1Z1, Canada*

(Received 16 November 2004; accepted 10 January 2005; published online 4 April 2005)

We investigate the *reentrant* onset of chaos in “tubular image states,” which are loosely bound states of electrons formed in the vicinity (20–40 nm) of conducting nanotubes. Chaos is shown to arise when an electron is placed in the vicinity of *two* metallic nanotubes with a magnetic field applied along the tubes. At stronger magnetic fields  $B \sim 10$  T, we observe the formation of Landau-like states encircling the two-tube system, which wipe out the chaos. We can *reinstall* the chaos by charging oppositely the nanotubes, thus breaking the symmetry of the system and correspondingly the shape of the Landau-like states. Detailed analysis of the onset of chaos is done by studying the statistical properties of the eigenvalues spectrum and by investigating the spatial autocorrelation functions of individual eigenstates. © 2005 American Institute of Physics.  
[DOI: 10.1063/1.1865932]

### I. INTRODUCTION

Much of the theoretical and experimental research on quantum chaos has been performed on Rydberg atoms in strong electric and magnetic fields.<sup>1</sup> For high enough fields, these systems undergo transitions from regular to chaotic behavior. This transition is indicated in the change in the statistics of the energy spectrum; the appearance of multiple avoided crossing; and the high sensitivity of energy eigenvalues to small external perturbations.<sup>2–5</sup> Analogous studies have been performed on quantum dots, where chaos can be introduced by applying magnetic fields on regular shaped dots or due to the electron scattering with the dot’s irregular boundaries.<sup>6</sup> Chaotic electron dynamics has also been explored in other nanostructures, such as antidots arrays,<sup>7</sup> resonant tunneling diodes,<sup>8</sup> quantum wells,<sup>9</sup> and superlattices.<sup>10,11</sup>

In this paper, we introduce a new type of quantum platform for the investigation of chaos on the *nanoscale*: that of image states formed when an electron hovers in the vicinity of suspended nanowires, such as metallic carbon nanotubes.<sup>12</sup> We have shown that these image states, named “tubular image states” (TIS), which extend some  $\sim 10$ – $50$  nm away from the tube’s surface, owe their stability to the existence of angular momentum barriers that largely delay the electron from collapsing on the surface.<sup>13</sup> In a recent experiment, the existence of TIS with *prolonged lifetimes* was reported in multiwall nanotubes.<sup>14</sup> Therefore, it is of interest to study TIS in other systems such as inhomogeneous nanowires<sup>15</sup> and nanowire arrays.<sup>16</sup>

Recently, we have also shown that in a single pair of parallel nanotubes TIS can be tuned by electric and magnetic fields, which could lead to the formation of chaos.<sup>17</sup>

Here, we thoroughly analyze the transition from regularity to chaos of the double-tube TIS in the presence of crossed electric and magnetic fields. In particular, we explore the *onset* and *disappearance* of chaos, as induced by the external fields. The analysis makes use of the statistics of the energy-levels distribution and the spatial behavior of autocorrelation functions for individual wave functions. These two indicators confirm and complement each other enabling us to explore the onset of chaos both as a property of the entire energy spectrum, and at the level of the individual eigenstate.

### II. THE MODEL SYSTEM

In Fig. 1, we depict the system under investigation.<sup>17</sup> It is comprised of two parallel metallic nanotubes of radius  $a$ , whose long axes are aligned along the  $z$  direction. The centers of the tubes are placed at  $x = \pm d/2, y = 0$ . We apply an external magnetic field  $\mathbf{B}$  oriented along the  $z$  direction. We also create an electric field directed in the  $x$ - $y$  plane, by positively charging one nanotube, thereby increasing its potential by  $V_a$ , and negatively charging the other, increasing its potential by  $-V_a$ .

We assume that the nanotubes are ideally conducting cylinders.<sup>12,18</sup> When an external electron is placed at a distance  $r$  from the center of a tube it creates an image charge to

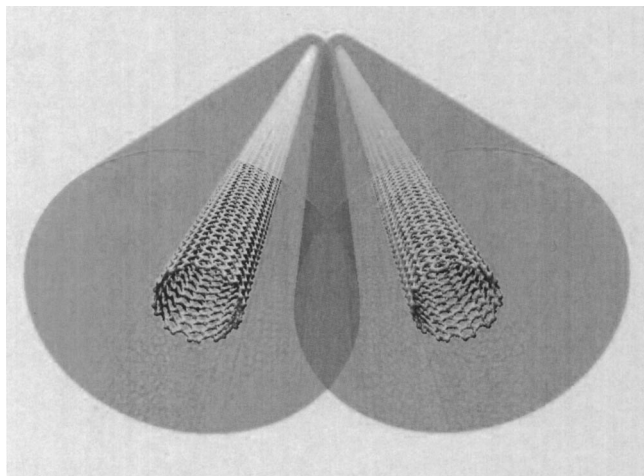


FIG. 1. Tubular image states of electron in the vicinity of two parallel nanotubes. The states are tuned by oppositely charging the tubes while applying a magnetic field directed along their long axis.

which it gets attracted. For an infinitely long tube, the screening potential felt by the electron due to the image charges can be approximated by<sup>12</sup>

$$V_s(r) \approx \frac{2e^2}{\pi a} \sum_{n=1,3,5,\dots} \text{li}[(a/r)^n], \quad \text{li}(x) \equiv \int_0^x \frac{dt}{\ln(t)}, \quad (1)$$

interpolating well between the long-range  $-e^2/[r \ln(r/a)]$  form and the near-surface  $1/|r-a|$  behavior.

In the charged two-tube system, an electron separated at the distance  $r_1$  and  $r_2$  from the centers of the two tubes, respectively, feels an additional potential due to the charging of the tubes, given as<sup>18</sup>

$$V_C(r_1, r_2) \approx eV_a \frac{\ln(r_1/r_2)}{\ln(a/d)}. \quad (2)$$

Here, we assume that the distance between the tubes  $d$  is much larger than their radii  $a$ , i.e.,  $d \gg a$ .  $V_C$  has the correct values of  $\pm eV_a$  when the electron is placed on the surface of one of the tubes, i.e., when  $r_1 = a$  and  $r_2 = d$  and *vice versa*. Neglecting the short-range cross-polarization terms arising from multiple reflections of image charges belonging to different nanotubes, the total potential energy of the external electron is

$$V_T(r_1, r_2) = V_s(r_1) + V_s(r_2) + V_C(r_1, r_2). \quad (3)$$

We also apply to the system a uniform magnetic field  $\mathbf{B}$  oriented along the  $z$  axis of the tubes. Then the total Hamiltonian of the image state electron is

$$H = \frac{1}{2m_e} (\mathbf{p} - e\mathbf{A})^2 + V_T(x, y), \quad (4)$$

where  $\mathbf{A} = B/2(-y, x, 0)$  is the vector potential of the field in the Landau gauge and  $\mathbf{p}$  is the generalized momentum of the electron. It gives rise to two additional terms in the Hamiltonian (4),

$$H_1 = -\frac{eB}{2m_e} L_z, \quad H_2 = \frac{e^2 B^2}{8m_e} (x^2 + y^2), \quad (5)$$

where  $L_z = -i\hbar[x(\partial/\partial y) - y(\partial/\partial x)]$  is the angular momentum operator and  $m_e$  is the electronic mass. In what follows we ignore the electronic spin.

The total wave function of the external electron is separable in the  $z$  coordinate,  $\Psi(x, y, z) = \psi_\nu(x, y) \phi_{k_z}(z)$ , hence its energy is given as  $E_\nu + \epsilon_{k_z}$ . The  $\psi_\nu(x, y)$  component obeys the Schrödinger equation

$$\left\{ \frac{-\hbar^2}{2m_e} \left( \frac{\partial^2}{\partial x^2} + \frac{\partial^2}{\partial y^2} \right) + V_T(x, y) + H_1(x, y) + H_2(x, y) \right\} \times \psi_\nu(x, y) = E_\nu \psi_\nu(x, y). \quad (6)$$

We solve Eq. (6), by using a multidimensional discrete variable representation algorithm.<sup>19</sup> In the following section we describe how the system's eigenstates depend on the applied electric and magnetic fields.

### III. THE SYSTEM EIGENERGIES

For large intertube separations  $d$  and in the absence of external fields, the low energy eigenstates are doubly degenerate, and the states in each doublet are localized around different tubes.<sup>17</sup> As  $d$  decreases, molecularlike states emerge, with the degeneracy between states of different parity being lifted, in direct analogy with the formation of *gerade* and *ungerade* states of homonuclear diatomic molecules.<sup>16</sup>

For weak magnetic fields, where  $B$  is a perturbation to  $V_T$ , these states become gradually modified by the (linear)  $H_1$  term, giving the Zeeman effect. As  $B$  gets stronger, the (non-linear)  $H_2$  term of Eq. (5) dominates. From Eq. (5), it is obvious that this turnover occurs at lower  $B$  for highly excited TIS,<sup>12</sup> which are more detached from the tubes. In the high- $B$  limit, Landau-like states of a free electron in an homogeneous magnetic field are formed, when  $V_T(x, y)$  may be neglected relative to  $H_2$ . Using cylindrical coordinates,  $\mathbf{r} = (\rho, \phi, z)$ , these tube-free eigenstates are given as

$$\Psi_{nlk}(\mathbf{r}) = e^{ikz} e^{il\phi} u_{nl}(\rho),$$

$$E_{nlk} = \frac{\hbar^2 k^2}{2m_e} + \frac{eB\hbar}{m_e} \left( n + \frac{1+l+|l|}{2} \right), \quad (7)$$

where  $u_{nl}(\xi) \propto \xi^{|l|/2} e^{-\xi/2} L_n^{|l|}(\xi)$ ,  $\xi = eB\rho^2/2\hbar$ , and  $L_n^{|l|}$  are the associated Laguerre polynomials,<sup>20</sup> with  $n=0, 1, 2, \dots$ ,  $l=0, \pm 1, \pm 2, \dots$ . As we turn on and further increase  $V_a$ , the Landau-like states get distorted, gradually losing their typical shape altogether.<sup>17</sup>

In Fig. 2 (left), we display the dependence of the system eigenenergies on the magnetic field  $B=0-35$  T for  $V_a=0$ . The tubes radii  $a=0.7$  nm and intertube separation  $d=40$  nm were used here and throughout the paper. We present here only the high energy states,<sup>17</sup>  $\nu=75-150$ , which are strongly affected by the magnetic field. For intermediate fields  $B < 10$  T, the system possesses a rather complex spectrum, which at higher fields  $B > 20$  T and quantum numbers  $\nu \geq 100$  becomes more regular, due to the appearance of the Landau-type states (see dashed lines), and also Fig. 4). In Fig.

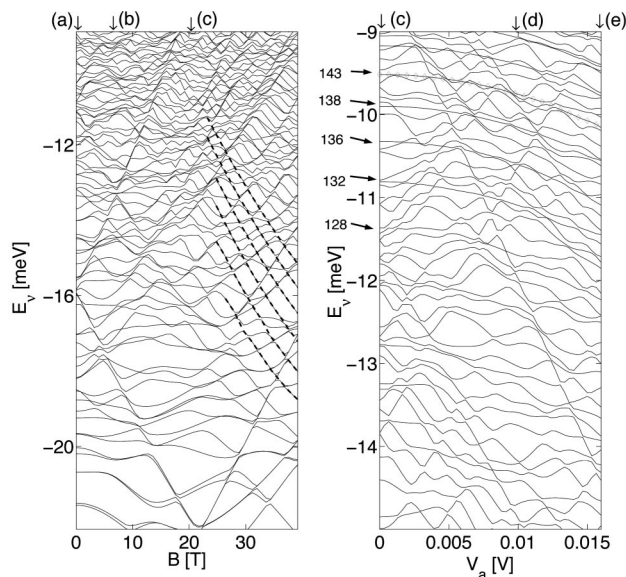


FIG. 2. (Left) Dependence of the eigenstates on the magnetic field  $B$  where  $V_a=0$ . We show eigenstates numbers 75–150. (Right) Dependence of the high energy states  $\nu=101$ –145 on  $V_a$  for  $B=20$  T. The  $\nu$  index designates the positions of the ( $V_a=0$ ) Landau-type states, where  $\nu=143$  is marked by diamonds.

2 (right), we show the higher eigenenergies for the  $B=20$  T case as a function of  $V_a$ .<sup>17</sup> We can follow a series of Landau-like states corresponding to ( $V_a=0$ )  $\nu=119, 128, 132, 136, 138, 143$ . As we increase  $V_a$ , their energies start to move down, accompanied by the collapse of the states on the right tube, see also Fig. 4. We also observe a large number of avoided crossings in the high  $V_a$  regime.

## IV. ANALYSIS OF THE ONSET OF CHAOS

### A. Level spacing distribution

We now analyze in details the onset of chaos in the above spectra. Most of the “generic” indicators of quantum chaos are based on multistate properties. Such are the indicators which examine the existence of avoided crossings,<sup>21</sup> the average level density,<sup>5</sup> and the level spacing fluctuations.<sup>2,22–24</sup> In particular, it is known that the level spacing distribution should change from a Poissonian type to a Wigner type for chaotic states which obey the eigenvalue statistics of Gaussian orthogonal ensembles.

In Fig. 3 we demonstrate that such transitions occur for TIS, as we turn on the magnetic and electric fields. We calculate the level statistics in the energy window  $-18 \text{ meV} \leq E_\nu \leq -9 \text{ meV}$  and display it for five situations from Fig. 2: The magnetic field is being increased from 0 to 20 T in cases (a)–(c). It is further accompanied by a growing electric field in (d) and (e). With the parameter  $\langle S \rangle$  being the average energy spacing, we find that in cases (a) and (c), the nearest-neighbor energy spacing distributions are clearly Poissonian,  $P \sim e^{-S}$ , indicating that the states are uncorrelated and the system is regular. In contrast, the other cases can be approximately described by the Wigner distribution  $P \sim \frac{1}{2} \pi S e^{-\pi S^2/4}$ , indicating chaotic dynamics. Specifically, the data could be well fitted to the Berry–Robnik distribution function<sup>24</sup>

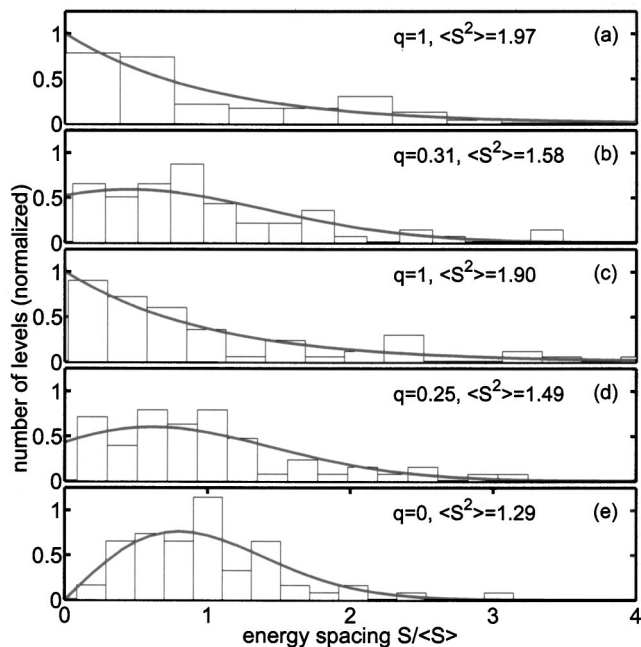


FIG. 3. Nearest-neighbor energy spacing histograms for states in the energy regime  $-18 \text{ meV} \leq E_\nu \leq -9 \text{ meV}$ . (a)  $B=0, V_a=0$ ; (b)  $B=6 \text{ T}, V_a=0$ ; (c)  $B=20 \text{ T}, V_a=0$ ; (d)  $B=20 \text{ T}, V_a=0.010 \text{ V}$ ; (e)  $B=20 \text{ T}, V_a=0.016 \text{ V}$ . These setups are marked by arrows at the top of Fig. 2. The smooth curves in the histograms are the Poisson (a), (c) and Wigner (e) distributions. The curves in (b), (d) are the result of a least square fit by Eq. (8) yielding  $q=0.31, q=0.25$ .

$$P(S, q) = [2q(1-q) + \pi(1-q)^3 S/2] e^{-qS - \frac{1}{4}\pi(1-q)^2 S^2} + q^2 e^{-qS} \text{erfc}[\sqrt{\pi}(1-q)S/2], \quad (8)$$

interpolating well between the Poisson ( $q=1$ ) and the Wigner ( $q=0$ ) distributions. Another indicator is the mean square level spacing  $\langle S^2 \rangle = \int_0^\infty P(S, q) S^2 dS$ , which should decrease from the value of 2 in the Poissonian case to  $4/\pi = 1.27$  for the Wigner distribution.<sup>24</sup> In Fig. 3 we again find that cases (a) and (c) are regular, while the other systems show an intermediate, (b) and (d), or fully chaotic dynamics (e).

These results of Fig. 3 show that in the absence of fields the system is regular (a), and it starts to become chaotic only as the magnetic field is turned on (b). However, for stronger magnetic fields (c) the chaotic features are eliminated by the formation of the Landau-like states. Only as we increase the electric field chaos reappears again (d,e). We have also verified, that the fitting parameter  $q$  systematically goes to zero as  $V_a$  is increased, demonstrating the smooth reappearance and domination of chaos. Note that the Wigner-like distribution observed in Fig. 3 agrees well with the strong anticrossing observed in Fig. 2 with a level repulsion of degree 1 as  $P(S) \sim S$  for  $S \rightarrow 0$ .<sup>23</sup>

In Fig. 4, we also reveal these transitions by showing typical states from the five regimes discussed in Fig. 3. Plot (a) displays a molecularlike state for the zero field situation. As the magnetic field is turned on, eigenstates become complicated and manifest chaotic features (b), in accordance with the transition from the Poisson to the Wigner distribution, as shown in Figs. 3(a) and 3(b). Only when the magnetic field is

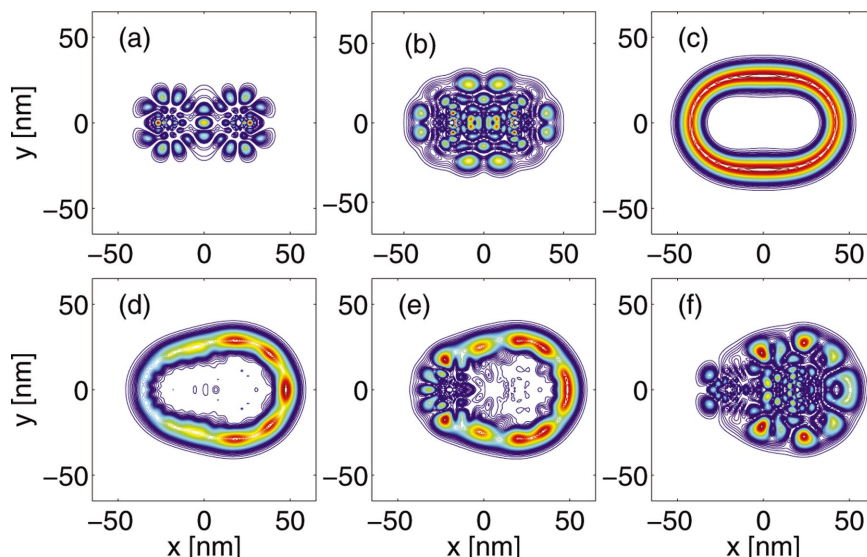


FIG. 4. (Color) Probability density for six representative states. In all cases  $d=40$  nm and the tubes are located at  $x=\pm 20$  and  $y=0$ . (a)  $B=0$  T,  $V_a=0$  V; (b)  $B=6$  T,  $V_a=0$  V; (c)  $B=20$  T,  $V_a=0$  V; (d)  $B=20$  T,  $V_a=8.5 \times 10^{-3}$  V; (e)  $B=20$  T,  $V_a=1.2 \times 10^{-2}$  V; (f)  $B=20$  T,  $V_a=1.6 \times 10^{-2}$  V. The frames (c)–(f) follow the  $\nu=143$  Landau-like state (marked by “diamonds” in Fig. 2) as the electric field is increased.

high enough ( $B > 10$  T), we observe the formation of regular Landau orbits (c), and reappearance of the Poissonian statistics. However, as the electric field  $V_a$  is turned on, the states first shift (d), then nest on one of the tubes (e), and finally develop chaotic nodal patterns (f).<sup>25</sup> This behavior is consistent with the proliferation of avoided crossings shown in Fig. 2 (Ref. 21) and related changes of the statistics in Figs. 3(c)–3(e).

We can compare the present system with other related problems. In particular, the TIS in a single-tube system are analogous to electronic states in a two-dimensional (2D) hydrogen atom model system;<sup>26</sup> both do not show chaos in magnetic fields. On the other hand, the TIS in the pair of nanotubes are analogous to states in a 2D hydrogenic molecule  $H_2^+$ . When the Landau states form in stronger magnetic fields, encircling both tubes at large distances, the system effectively behaves again like a 2D hydrogen atom, with no signs of chaos. This transition is disturbed by the application of the electric field, so that we obtain again “molecular” features, accompanied by the reentrance of chaos.

From this discussion it is also obvious that chaos should be a property of a group of states in a certain energy interval. This behavior is demonstrated in Fig. 5, for the system at  $B=20$  T and  $V_a=0.016$  V, by studying the nearest-neighbors energy spacing distribution at different energy intervals. We find that the low-energy states, located around individual tubes, are mostly regular, since  $q=0.71$  and  $\langle S^2 \rangle=1.84$  (a). In the intermediate energy regime, where the orbit sizes are comparable to  $d$ , chaos predominates,  $q=0$  and  $\langle S^2 \rangle=1.30$  (b). Only as we go to higher energies, where the very high Landau-like states encircle both tubes, the system partly recovers its regular behavior, and  $q=0.38$  and  $\langle S^2 \rangle=1.62$  (c).

## B. Autocorrelation functions of the wave functions

We have seen above in Fig. 5 that chaos is localized in certain regions of energy eigenstates. Its dominance was

identified through multistate properties. We could thus naturally ask if one can study and characterize the onset of chaos from *single* energy eigenstates.<sup>27</sup> In analogy with classical chaos, which is commonly associated with randomness and the decay of correlations, one looks here at the decay of an autocorrelation function built from the wave function itself. Such an autocorrelation function can be defined<sup>27</sup> as

$$F(\delta) = \int \psi^*(\mathbf{q}) \psi(\mathbf{q} + \delta) d\mathbf{q}. \quad (9)$$

Here the  $\mathbf{q}$  integration is performed over a self-avoiding space-filling path. In the present application, the  $\delta$  displacement vector is also directed along this path. The discrete version of this expression is

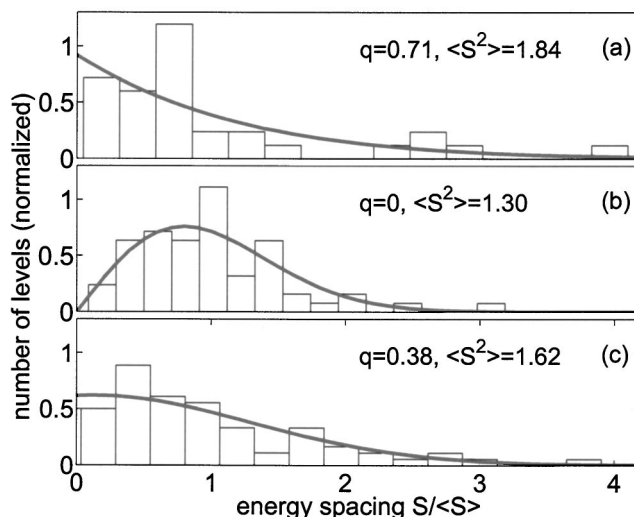


FIG. 5. Nearest-neighbor energy spacing histograms for the  $B=20$  T,  $V_a=0.016$  V system for different energy intervals. (a)  $-29$  meV  $\leq E_\nu \leq -18$  meV; (b)  $-18$  meV  $\leq E_\nu \leq -9.5$  meV; (c)  $-9.5$  meV  $\leq E_\nu \leq -5.5$  meV. The smooth curves in the histograms are the result of a least square fit by Eq. (8).

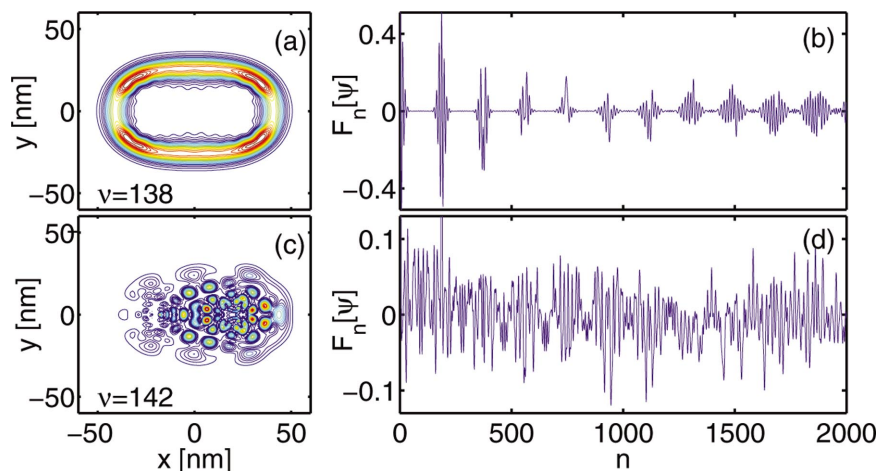


FIG. 6. (Color) The real part of  $F_n[\Psi]$  for a pair of regular and chaotic states. (a) Probability density of a regular state formed when  $B=20$  T and  $V_a=0$ . (b) The corresponding correlation function. (c) The probability density of a chaotic state formed when  $B=20$  T and  $V_a=0.009$  V. (d) The corresponding correlation function.

$$F_n[\psi] = \frac{1}{N} \sum_{i=1}^N \psi^*(r_i) \psi(r_{i+n}), \quad n \leq N, \quad (10)$$

where  $r_1, r_2, \dots, r_N$  is a cyclic ( $r_{N+n}=r_n$ ) set of ordered points belonging to the self-avoiding space-filling path.

According to the indicator proposed in Ref. 27 a wave function  $\psi$  is termed chaotic if its autocorrelation function is aperiodic and rapidly decaying. In our case, since the TIS wave functions are complex, due to the arbitrary gauge choice, the autocorrelation function has an additional imaginary part. In Fig. 6 we demonstrate the behavior of  $F_n[\Psi]$  in two extreme cases: (a) a  $V_a=0$  “regular” state with  $B$  set at 20 T; (c) an “irregular” state obtained when both  $B$  and  $V_a$  are nonzero. The autocorrelation function shows nearly periodic features in the first case (b). In contrast it very rapidly decays while fluctuating about zero, for the irregular state (d). In both cases, we magnify the values of  $F_n[\Psi]$ , which is normalized to 1 at  $\delta=0$ .

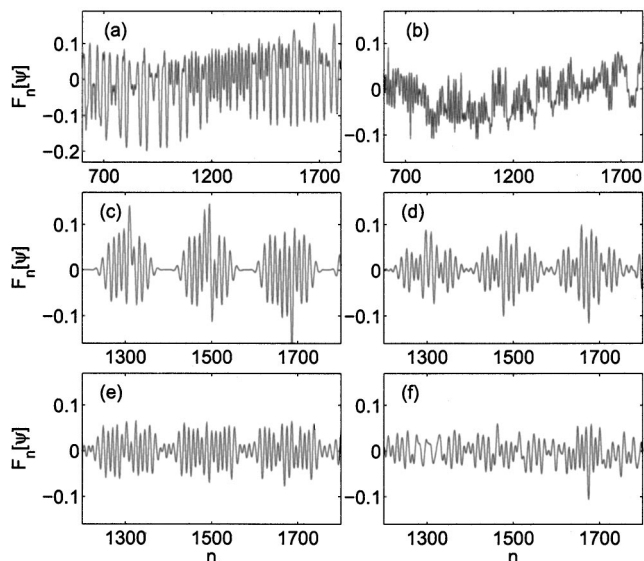


FIG. 7. The real part of the autocorrelation function  $F_n[\Psi]$  for the corresponding (a)–(f) states shown in Fig. 4.

We have calculated  $F_n[\Psi]$  also for the sequence of representative states plotted in Fig. 4, as shown in Fig. 7. We find that there is indeed a very strong correlation between the statistical properties of the states, viewed in Fig. 3, the visual distortion of the state as viewed in Fig. 4 and the disappearance of the periodic features of the autocorrelation function. Erratic sequences of oscillations in  $F_n[\Psi]$  are obtained either when the magnetic field is weak  $B=6$  T, or when a strong magnetic field is combined with high electric field. We have also checked that different constructions of the path lead basically to the same observations.

## V. SUMMARY

We have shown that tubular image states formed above pairs of nanotubes can become chaotic in the presence of magnetic and electric fields. We have characterized chaos by the energy spectrum statistics and by the properties of individual states. These studies reveal that the present system manifests several regimes with an unusual *reentrant* onset of chaos. This behavior can be addressed to the special character of this system, combining features of nanoscale, molecular, and Rydberg-atom systems. We expect that other phenomena could be traced in these fascinating systems, when more nanotubes are included, which could lead to novel potential applications.

## ACKNOWLEDGMENTS

The authors gratefully acknowledge numerous discussions with P. Brumer. This project was supported by a grant from the Feinberg graduate school of the WIS.

<sup>1</sup>G. Casati and B. Chirikov, *Quantum Chaos* (Cambridge University Press, New York, 1995).

<sup>2</sup>G. Wunner, U. Woelk, I. Zech, G. Zeller, T. Ertl, F. Geyer, W. Schweitzer, and H. Ruder, *Phys. Rev. Lett.* **57**, 3261 (1986).

<sup>3</sup>C. Neumann, R. Ubert, S. Freund, E. Flöthmann, B. Sheehy, K. H. Welge, M. R. Haggerty, and J. B. Delos, *Phys. Rev. Lett.* **78**, 4705 (1997).

<sup>4</sup>J. von Milczewski and T. Uzer, *Phys. Rev. E* **55**, 6540 (1997).

<sup>5</sup>F. Haake, *Quantum Signatures of Chaos* (Springer, Berlin, 2000).

<sup>6</sup>Y. Alhassid, *Rev. Mod. Phys.* **72**, 895 (2000).

- <sup>7</sup>D. Weiss, M. L. Roukes, A. Menshig, P. Grambow, K. von Klitzing, and G. Weimann, *Phys. Rev. Lett.* **66**, 2790 (1991).
- <sup>8</sup>T. M. Fromhold, L. Eaves, F. W. Sheard, M. L. Leadbeater, T. J. Foster, and P. C. Main, *Phys. Rev. Lett.* **72**, 2608 (1994).
- <sup>9</sup>T. M. Fromhold, P. B. Wilkinson, F. W. Sheard, L. Eaves, J. Miao, and G. Edwards, *Phys. Rev. Lett.* **75**, 1142 (1995).
- <sup>10</sup>T. M. Fromhold, A. A. Krokhin, C. R. Tench, S. Bujkiewicz, P. B. Wilkinson, F. W. Sheard, and L. Eaves, *Phys. Rev. Lett.* **87**, 046803 (2001).
- <sup>11</sup>T. M. Fromhold, A. Patane, S. Bujkiewicz *et al.*, *Nature (London)* **428**, 726 (2004).
- <sup>12</sup>B. E. Granger, P. Král, H. R. Sadeghpour, and M. Shapiro, *Phys. Rev. Lett.* **89**, 135506-1 (2002).
- <sup>13</sup>D. Segal, P. Král, and M. Shapiro, *Surf. Sci.* **577**, 86 (2005).
- <sup>14</sup>M. Zamkov, N. Woody, B. Shan, H. S. Chakraborty, Z. Chang, U. Thurmm, and P. Richard, *Phys. Rev. Lett.* **93**, 156803-1 (2004).
- <sup>15</sup>D. Segal, P. Král, and M. Shapiro, *Phys. Rev. B* **69**, 153405 (2004).
- <sup>16</sup>D. Segal, B. E. Granger, H. R. Sadeghpour, P. Král, and M. Shapiro, *Phys. Rev. Lett.* **94**, 016402 (2005).
- <sup>17</sup>D. Segal, P. Král, and M. Shapiro, *Chem. Phys. Lett.* **392**, 314 (2004).
- <sup>18</sup>J. C. Slater and N. H. Frank, *Electromagnetism* (McGraw-Hill, New York, 1947).
- <sup>19</sup>D. T. Colbert and W. H. Miller, *J. Chem. Phys.* **96**, 1982 (1992).
- <sup>20</sup>L. D. Landau and E. M. Lifshitz, in *Quantum Mechanics*, Nonrelativistic Theory Vol. 3 (Butterworth-Heinemann, UK, 1998).
- <sup>21</sup>B. V. Chirikov, *J. Stat. Phys.* **3**, 307 (1971).
- <sup>22</sup>S. W. McDonald and A. N. Kaufman, *Phys. Rev. Lett.* **42**, 1189 (1979).
- <sup>23</sup>O. Bohigas, M. J. Giannoni, and C. Schmit, *Phys. Rev. Lett.* **52**, 1 (1984).
- <sup>24</sup>M. V. Berry and M. Robnik, *J. Phys. A* **17**, 2413 (1984).
- <sup>25</sup>R. M. Stratt, N. C. Handy, and W. H. Miller, *J. Chem. Phys.* **71**, 3311 (1979).
- <sup>26</sup>X. L. Yang, S. H. Guo, F. T. Chan, K. W. Wong, and W. Y. Ching, *Phys. Rev. A* **43**, 1186 (1991).
- <sup>27</sup>M. Shapiro and G. Goelman, *Phys. Rev. Lett.* **53**, 1714 (1984).